Thermomechanical Properties of the Crystal Phase of Poly(ethylene terephthalate) by Molecular Modeling

Gregory C. Rutledge

Department of Chemical Engineering, Massachusetts Institute of Technology, Cambridge, Massachusetts 02139

Received December 9, 1996; Revised Manuscript Received February 12, 1997[⊗]

ABSTRACT: Theoretical values for the thermomechanical properties of poly(ethylene terephthalate) (PET) are determined self-consistently using the pcff force field to compute the potential energy and quasiharmonic lattice dynamics to determine the vibrational free energy. Complete sets of lattice constants, thermal expansion coefficients, elastic properties, and Grüneisen coefficients are reported between 0 and 400 K for the triclinic PET unit cell. Mean square displacement matrices for the constituent atoms of PET were determined, from which a theoretical *B*-factor for X-ray scattering of 4.0 Å^2 at 300 K is estimated. The 50% probability ellipsoids for thermal vibration of all atoms in the asymmetric unit are computed. Calculated lattice parameters at 300 K agree with experimental data, to within the accuracy of the method. Calculated elastic constants for a transverse isotropic composite agree with data from X-ray and ultrasonic velocity measurements on highly oriented samples. The tensile elastic stiffness constants are temperature-dependent, while the shear stiffnesses are roughly constant in the range 0−400 K. Thermal contraction along the chain direction is observed in PET, consistent with results for other polymer crystals possessing chains in fully extended conformations. The driving force for contraction is entropic in origin, arising from negative γ_3 and γ_6 Grüneisen coefficients.

Introduction

Poly(ethylene terephthalate) (PET) is an industrially important polymer in both fiber and film form, in large part due to its attractive mechanical properties. PET is known to exhibit a complex multiphase morphology consisting of both crystalline and noncrystalline phases. The crystalline phase may contribute highly anisotropic behavior to the bulk polymer due to the orientation of chains which accompanies preferential alignment of the crystallites themselves; such preferential alignment may be accomplished through careful processing operations. The noncrystalline phase is also often anisotropic, prompting investigators to decompose this component into isotropic and oriented constituents.[1,2] In some instances, the oriented component is described as a spatially distinct component, such as an interphase between crystalline and isotropic regions; alternatively, it may be considered to be composed of predominantly extended conformers intimately mixed with the isotropic component of the amorphous phase. The degree of orientation in the noncrystalline component may also be manipulated through processing, leading to a range of mechanical behavior manifested in fibers and films.

Given the level of morphological complexity exhibited by PET, it is a difficult problem to deconvolute empirically the contributions of each component to the overall behavior observed in the macroscopic sample. Molecular modeling offers one avenue around this problem. Well-controlled, pure crystalline and noncrystalline components may be examined individually by construction of the model. Furthermore, a comprehensive and self-consistent set of material properties, such as the elastic stiffness tensor, may be determined, including those components of the tensors which are difficult or impossible to measure experimentally. However, to our knowledge, no such comprehensive study of thermomechanical properties has been reported for PET. It is especially important in aromatic polymers and crystals of low symmetry to quantify the full tensorial nature of the stress−strain−temperature relationships; single-chain calculations may neglect important intermolecular interactions, and coupling of deformations along different axes can be significant. Furthermore, the computation of the temperature dependence of the properties of the crystal phase is also practical and can provide important corroborative tests of the calculations where such experimental data are available. In this communication we report the theoretical stress−strain response of the pure crystalline component of PET and its sensitivity to changes in temperature and orientation distribution of crystallites. Ultimately, we think such information may be used in combination with similar estimates for the other phase(s) to provide quantitative models for semicrystalline PET.

Computational Method

A self-consistent form of lattice dynamics is used to compute the free energy of the PET crystal, starting from only an empirical force field for valence and nonbonded interatomic interactions and a reasonable guess for the crystal structure. The force field employed here is the pcff force field, available with the Discover software of Biosym-MSI.[3] This force field has been parameterized specifically for aromatic esters by Sun.[4] The valence portion of the force field includes quartic bond stretch and bond angle bending terms, a three-term cosine expansion for torsions, bond−bond, bond−angle, angle−angle, bond-torsion, and angle-torsion cross terms, and inversion terms. The nonbonded portion of the force field is a 9−6 potential with Coulombic interactions for partial atomic charges. The valence force field was parameterized based on fitting to energies, first and second derivatives of energy, and electrostatic potentials from extensive *ab initio* quantum mechanical calculations using the 6−31G* basis set, and hence is derived from “first principles”, in a sense. The partial atomic charges employed are those recommended by the bond contribution approach in the pcff force field for PET and are summarized in Table 1. Concern regarding the ability of the pcff force field to predict correctly the gauche−trans ratio about the

[⊗] Abstract published in *Advance ACS Abstracts,* April 1, 1997.

Table 1. Partial Atomic Charges Assigned to Atoms of PET (in Units of Electron Charge)

atom type	partial atomic charge	isotropic B-factor (Å^2)
C (sp^3)	+0.119	3.1
C (carbonyl)	+0.720	2.8
C (arom, 1,4)	−0.127	2.5
C (arom, 2,3)	−0.018	3.1
H (aliphatic)	+0.053	5.7
H (aromatic)	+0.127	5.0
O (ether)	−0.396	3.4
O (carbonyl)	−0.531	4.0

Table 2. Calculated and Experimental Lattice Parameters and Density for PET

	0 K	100 K	200 K	300 K	400 K	exp[a] (300 K)
a (Å)	4.428	4.432	4.457	4.483	4.515	4.56
b (Å)	5.993	5.997	6.008	6.022	6.045	5.94
c (Å)	10.880	10.876	10.866	10.857	10.841	10.75
α (deg)	103.3	103.2	102.8	102.5	102.1	98.5
β (deg)	120.3	120.0	119.9	119.8	119.5	118
γ (deg)	106.8	106.9	107.0	107.0	107.1	112
ρ_T (g/cm^3)	1.499	1.491	1.475	1.456	1.432	1.455

[a] Reference 8.

carbon−carbon torsion of the ethylene unit in PET is not an issue here, since only small deviations from the trans conformer are relevant to the crystal phase. A dielectric constant of unity is assumed for these calculations. Ewald summations[5] are used to evaluate long-range dispersion and Coulombic interactions.

In this lattice dynamic computation, the state of lowest Gibbs free energy is determined by minimizing the total free energy with respect to both atomic position and lattice geometry. The total free energy is computed within the quasiharmonic approximation and comprises contributions from the ground state electronic energy, $U(\mathbf{a})$, the quantum mechanical vibrational free energy, $A_{vib}(T,\mathbf{a})$, and a work term due to deformation at fixed applied stress, as shown in eq 1. $\mathbf{a}$ is the set of lattice vectors, V_T is the equilibrium volume of the unit cell at temperature T, and σ and ϵ are the 6 × 1 vectors for stress and strain, respectively, in Voigt notation. (The superscript "t" is used to denote the vector transpose.)

$$G(T,\sigma) = U(\mathbf{a}) + A_{vib}(T,\mathbf{a}) - V_T\sigma^t\epsilon \qquad (1)$$

$$A_{vib} = \frac{\int_{BZ}\mathrm{d}\mathbf{k}\sum_j^{3N_a}\frac{\hbar\omega_j(\mathbf{k})}{2} + k_BT\ln\left(1-\exp\left[\frac{-\hbar\omega_j(\mathbf{k})}{k_BT}\right]\right)}{\int_{BZ}\mathrm{d}\mathbf{k}} \qquad (2)$$

Procedurally, the potential energy is first minimized with respect to atomic coordinates for a given set of lattice vectors, $\mathbf{a}$. At this minimum, the vibrational contribution to free energy is computed analytically using eq 2. The integration is approximated as a summation over the $3N_a$ normal mode vibrational frequencies, $\omega_j(\mathbf{k})$, computed in this case at 216 $\mathbf{k}$ points in the first Brillouin zone, using Gauss−Legendre quadrature. The calculation of A_{vib} neglects terms higher than second order in the Taylor series expansion of the potential energy surface about the local minimum. The resulting harmonic potential energy surface and vibrational frequencies are dependent upon the lattice vectors, thereby incorporating anharmonic effects due to volume and shape changes. The lattice vectors are then varied and the free energy recomputed to determine the structure of lowest Gibbs free energy. The resulting free energy optimum exhibits lattice parameters and vibrational frequencies fully consistent with the input force field; no experimental data are required to fix these quantities. Quantum mechanical effects, which are important for vibrational motion with frequencies $\omega > kT/\hbar$ (~200 cm^{-1} at room temperature), constituting the vast majority of phonons in molecular crystals, are accounted for. Most previous simulations of crystal properties have neglected thermal expansion, Poisson effects, vibrational entropy, quantum effects, or some combination of these. Further details of the calculational method and the relative importance of these different aspects have been reported elsewhere.[6] An analysis of the limitations of the quasiharmonic approximation and of perturbative corrections has also been presented previously.[7]

Results

(a) Lattice Dimensions and Thermal Vibration. The crystal structure used as a starting point for the calculations is that originally proposed by Daubeny et al.[8] This unit cell is triclinic. There is one repeat unit per unit cell. The experimentally determined lattice parameters are shown in Table 2. The calculations allow for full variability of the triclinic lattice, resulting in a total of six lattice degrees of freedom, one degree of freedom for the chain setting angle, and $3N_a - 6 = 60$ internal degrees of freedom.

A structure of minimum free energy was found in good agreement with that of Daubeny et al. Additional structures of comparable free energy were also identified, but were not studied in detail. Table 2 shows the lattice parameters and setting angles for the calculated structure at several temperatures from 0 to 400 K. At 300 K, the discrepancy in lattice parameters is <2% for all lengths and <5% for all angles. The computed density is remarkably close to that reported by Daubeny et al. This close agreement is actually at odds with much of our previous experience, where the use of a fully consistent lattice dynamic calculation and quantized normal mode vibrations, in combination with a potential energy surface computed with classically derived force fields, usually leads to a 1−4% expansion of the computed lattice over what is observed experimentally. Other researchers[9,10] have reported PET densities as much as 5% higher than that reported by Daubeny, which would be consistent with this trend. The reason for this underprediction, as has been discussed previously,[6,11] may be traced to the manner in which van der Waals parameters are derived for molecular mechanics force fields; this usually involves the use of classical static structure calculations, i.e. 0 K without explicit treatment of zero-point vibrations, to derive force field parameters which reproduce empirical data collected at finite temperatures. Comparing the computed vibrational frequencies with 40 experimentally observed IR and Raman frequencies ranging from 145 to 3085 cm^{-1}, reported and indexed by Boerio et al.,[12] indicates a root mean square deviation on the order of 35 cm^{-1}.

Figure 1 illustrates a diagram of the computed unit cell for PET at 300 K. The theoretical 50% probability ellipsoids for anisotropic thermal vibration are shown for the atoms of a reference chain in the unit cell. These are computed using eq 3 and sampling the dispersion curves in the first Brillouin zone of the reciprocal lattice.[14] For purposes of computing the mean square

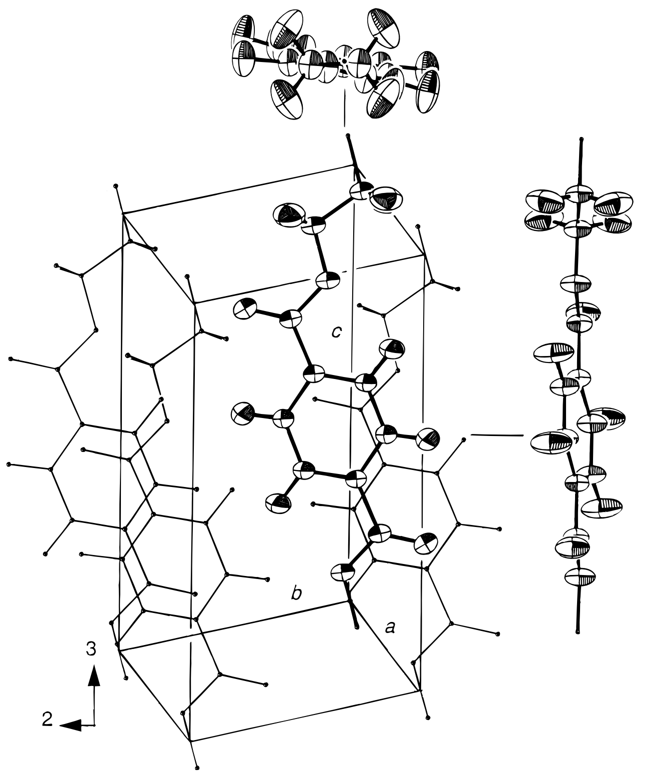

Figure 1. (a) Unit cell of PET, viewed along the 1-axis of the orthogonal axis system used for reporting properties. Illustrated for one chain are the 50% probability thermal vibration ellipsoids for each atom, computed from 216 normal mode vibrations in the first Brillouin zone. Also shown are three orthogonal views of the thermal vibration ellipsoids for the PET chain. The thermal vibration ellipsoids were plotted using Ortep-III.[13]

atomic displacement matrices, $\langle \mathbf{u}_i \mathbf{u}_i^t \rangle$, each normal mode is treated as an independent harmonic oscillator, with amplitude $E_{\mathrm{vib},j}(\mathbf{k})/\omega_j(\mathbf{k})^2$. $E_{\mathrm{vib},j}(\mathbf{k})$ is the energy of the jth vibration mode for wave vector $\mathbf{k}$, which is computed quantum mechanically using eq 4. $\omega_j(\mathbf{k})$ is the frequency for that mode. The atomic displacements are described by the polarization vector, $\xi_{i,j}(\mathbf{k})$, for atom i in mode j:

$$\langle \mathbf{u}_i \mathbf{u}_i^t \rangle_j = \frac{1}{N_a m_i} \int_{BZ} \frac{E_{\mathrm{vib},j}(\mathbf{k})}{\omega_j^{\,2}(\mathbf{k})} \xi_{i,j}(\mathbf{k}) (\xi^*_{i,j}(\mathbf{k}))^t \quad (3)$$

$$E_{\mathrm{vib},j}(\mathbf{k}) = \hbar\omega_j(\mathbf{k}) \left\{ \frac{1}{2} + \left[\exp\left(\frac{\hbar\omega_j(\mathbf{k})}{k_B T} \right) - 1 \right]^{-1} \right\} \quad (4)$$

From the mean square displacement matrix it is possible determine the atom-specific anisotropic temperature factors and their effect on the intensity of Bragg scattering in the theoretical X-ray diffraction pattern, without resort to empirical fitting. Inspection of Figure 1 confirms the physically intuitive picture of ring libration and CH_2 wag in PET. In polymer crystallography it is common to assume a uniform isotropic temperature factor for all atoms. The so-called B-factor for each atom may be estimated as $8\pi^2(\mathrm{trace}\langle \mathbf{u}_i \mathbf{u}_i^t \rangle)$; these values are shown in Table 1 and reveal a spread of roughly a factor of 2 between highest and lowest values. Averaging over all the atoms provides an estimate of 4.0 Å^2 for the B-factor of PET at 300 K. This value is comparable to those commonly used in analyses of experimental X-ray data for polymers. It may also be compared to the value of 9 Å^2 used by Daubeny et al. Limitations of the lattice dynamic theory have been estimated to cause underprediction of the B-factor by 5−10% at 300 K;[14] the higher value required for experimental analysis in this case may be interpreted as indicative of significant contributions from crystal imperfections.

In molecular crystals it is often expedient to treat the molecule (in this case the repeat unit of the chain) as a rigid body. By so doing, contributions to thermal displacement due to low-frequency lattice modes are retained, while high-frequency internal vibration modes are neglected. For purposes of comparison, the mean square amplitude of the rigid body displacement of the PET chain was determined by a least squares fit of the atomic displacements to a set of translation (**T**), libration (**L**), and coupled translation−libration (**S**) matrices as described by Willis and Pryor.[14] The diagonal elements of the rigid body displacement matrix are indicative of translational (T_{11}, T_{22}, and T_{33}) and librational (L_{11}, L_{22}, and L_{33}) motion of the chain about three mutually orthogonal axes. In this study, the orthogonal axes are related to the triclinic PET unit cell as follows: the 3-axis corresponds to the chain direction (c-axis); the 2-axis is at right angles to this and lies in the bc-plane; the 1-axis is then chosen to define a right-handed system and corresponds to the reciprocal lattice vector $\mathbf{a}^*$. This axis system is illustrated in Figure 1. Values for **T**, **L**, and **S** are shown in eq 5. The calculated values are consistent with oscillations of the chain predominantly lateral to and along the chain axis, and librational motion of the chain about the chain axis. (The components of **T** are in units of Å^2, the components of **S** in units of Å.)

$$\begin{bmatrix} \mathbf{T} & \mathbf{S} \\ (\mathbf{S}^*)^t & \mathbf{L} \end{bmatrix} = \begin{bmatrix} \begin{bmatrix} 4.89 & -0.18 & 0.14 \\ & 3.36 & -0.04 \\ & & 2.44 \end{bmatrix} & \begin{bmatrix} <10^{-2} & 0.11 & 0.05 \\ -0.12 & <10^{-2} & -0.01 \\ <10^{-2} & <10^{-2} & <10^{-2} \end{bmatrix} \\ & \begin{bmatrix} 0.08 & <10^{-2} & 0.03 \\ & 0.08 & 0.14 \\ & & 1.39 \end{bmatrix} \end{bmatrix} \times 10^{-2} \quad (5)$$

(b) Elastic Constants. The full isothermal elastic stiffness matrices for PET were computed at 50 K intervals from 0 to 400 K. In continuum elasticity, the elastic properties are conveniently referred to orthogonal axes. For consistency in reporting elastic properties, the triclinic PET unit cell is again referred to the set of orthogonal axes described in the previous section. The elastic stiffnesses C_{ij} (in Voigt notation) were estimated by imposing small but finite strains on the crystal lattice and computing the energy of deformation. From these calculations the second derivatives of Helmholtz free energy are estimated, and the elastic stiffnesses determined using eq 6. Deformation was confirmed to be linearly elastic for deformations below 0.8%. Values reported here are based on deformations of 0.5% for all strains except those involving extension along the chain direction, where deformations of 0.3% were used (0.2% at T > 300 K). All of the resulting elastic stiffness matrices were positive definite and elastically stable. The 21 independent elements computed for the full isothermal elastic stiffness matrices for the PET lattice at 100 K intervals between 0 and 400 K are shown in Table 3.

$$C_{ij}^T = \frac{1}{V_T} \left[\frac{\partial^2 A}{\partial \epsilon_i \partial \epsilon_j} \right]_{T,\epsilon_{k \neq i,j}} \quad (6)$$

Table 3. Isothermal Elastic Stiffnesses Calculated at Several Temperatures, Transverse Isotropic Averages at 300 K, and Comparison to Experiment[a]

	0 K	100 K	200 K	300 K	400 K	transverse isotropy at 300 K: Reuss ave	transverse isotropy at 300 K: Voigt ave	exp[b] (300 K)
C_{11} (GPa)	19.0	17.9	16.1	14.4	12.0	11.0	14.1	7.70
C_{22} (GPa)	22.8	21.3	19.2	17.3	15.1	(=C_{11})	(=C_{11})	(=C_{11})
C_{33} (GPa)	203.9	199.3	190.8	178.0	123.9	168	178	18.8, 110,[c] 118[d]
C_{44} (GPa)	6.6	6.6	6.4	6.6	6.4	1.9	4.0	1.62
C_{55} (GPa)	1.2	1.1	1.1	1.4	1.5	(=C_{44})	(=C_{44})	(=C_{44})
C_{66} (GPa)	1.1	1.1	1.1	1.2	1.2	0.9	2.9	1.12
C_{12} (GPa)	9.1	8.5	7.5	6.4	5.0	(=$C_{11} - 2C_{66}$)	(=$C_{11} - 2C_{66}$)	(=$C_{11} - 2C_{66}$)
C_{13} (GPa)	−0.1	0.6	1.7	3.4	8.9	3.4	6.4	5.07
C_{23} (GPa)	11.4	10.7	9.9	9.5	9.5	(=C_{13})	(=C_{13})	(=C_{13})
C_{14} (GPa)	−2.4	−2.3	−2.2	−2.2	−1.9	0	0	0
C_{24} (GPa)	5.0	4.4	3.9	3.3	2.8	0	0	0
C_{34} (GPa)	6.5	5.7	4.8	3.8	2.7	0	0	0
C_{15} (GPa)	−0.4	−0.3	−0.3	−0.3	−0.4	0	0	0
C_{25} (GPa)	−0.3	−0.4	−0.4	−0.5	−0.6	0	0	0
C_{35} (GPa)	0.0	−0.2	−0.7	−0.7	−1.9	0	0	0
C_{45} (GPa)	0.6	0.5	0.3	0.2	0.2	0	0	0
C_{16} (GPa)	−2.3	−2.2	−1.9	−1.8	−1.6	0	0	0
C_{26} (GPa)	1.2	1.1	0.9	0.5	0.5	0	0	0
C_{36} (GPa)	−0.8	−0.8	−1.1	−1.8	−3.7	0	0	0
C_{46} (GPa)	0.0	0.0	−0.3	−0.4	−0.4	0	0	0
C_{56} (GPa)	0.0	0.0	0.0	0.0	−0.2	0	0	0

[a] Theoretical values accurate to approximately ±0.5 GPa. [b] Reference 16. [c] Reference 10. [d] Reference 17.

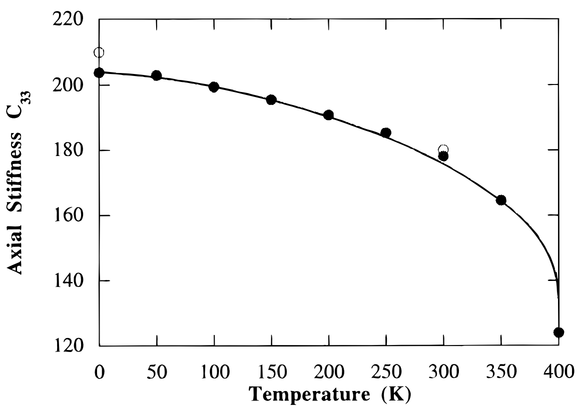

Figure 2. Axial stiffness C_{33} for the PET crystal as a function of temperature. Filled symbols are direct calculations of C_{33}. Open symbols at 0 and 300 K were determined indirectly by inversion of the computed compliance matrix.

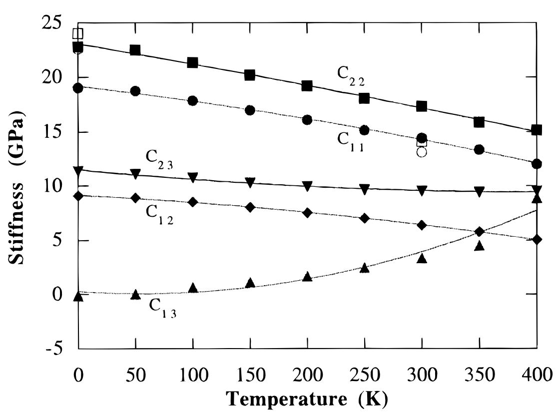

Figure 3. Transverse stiffnesses for the PET crystal as functions of temperature: C_{11} (circles); C_{22} (squares); C_{12} (diamonds); C_{13} (triangles); C_{23} (inverted triangles). Filled symbols are direct calculations of C_{ij}. Open symbols at 0 and 300 K were determined indirectly by inversion of the computed compliance matrix.

Several principal components of the elastic stiffness tensor are plotted as a function of temperature in Figures 2−4. These values were checked by computing the full elastic compliance matrix **S** at 0 and 300 K using

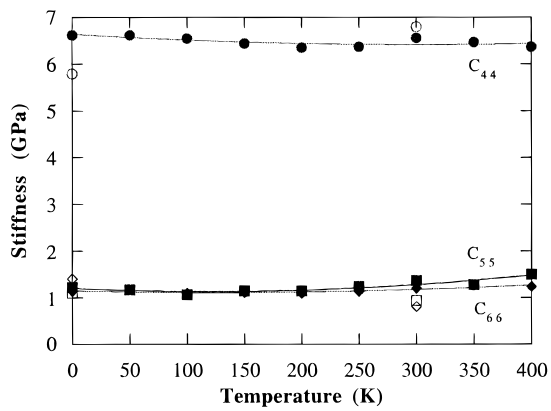

Figure 4. Shear stiffnesses for the PET crystal as functions of temperature: C_{44} (circles); C_{55} (squares); C_{66} (diamonds). Filled symbols are direct calculations of C_{ii}. Open symbols at 0 and 300 K were determined indirectly by inversion of the computed compliance matrix.

finite stresses of 50 (σ_1, σ_2), 350 (σ_3), and 20 MPa (σ_4, σ_5, σ_6) and recomputing the strained lattice of minimum free energy, to get $S_{ij} = \partial\epsilon_i/\partial\sigma_j$. These latter values are more prone to numerical error, but the resulting compliance matrices may nevertheless be inverted to yield the corresponding stiffness matrices $\mathbf{C} = \mathbf{S}^{-1}$. The diagonal elements C_{ii} determined in this manner are also plotted in Figures 2−4 and are consistent with the elastic stiffnesses computed directly.

Using relations[15] for computing the average compliance matrix corresponding to fiber symmetry under homogeneous stress (Reuss average) and homogeneous strain (Voigt average) conditions, theoretical bounds on the elastic stiffness matrix for a transverse isotropic, fully crystalline PET at 300 K were determined. These are also shown in Table 3, where they are compared to the experimental measurements by Hine and Ward using hot-compacted PET fiber specimens.[16] For the most part, the experimentally observed elastic stiffnesses are comparable to or less than the theoretical Reuss averages. In general, the discrepancies may be attributed to the imperfect crystallinity and orientation of crystallites in the hot-compacted PET sample. This is certainly true in the case of fiber axial stiffness C_{33},

Table 4. Young's Moduli, Shear Moduli, Poisson's Ratios, and Compressibilities for PET Calculated at 300 K under Conditions of Transverse Isotropy and Comparison to Experiment

	transverse isotropy at 300 K		
	Reuss ave	Voigt ave	exp[a] (300 K)
E_1, E_2 (GPa)	3.4	9.32	3.70
E_3 (GPa)	167	174	14.9, 110,[b] 118[c]
G_1, G_2 (GPa)	2.0	4.0	1.62
ν_{12}	0.83	0.57	0.65
ν_{13}, ν_{23}	0.17	0.29	0.39
χ (GPa^{-1})	0.102	0.91	na

[a] Reference 16. [b] Reference 10. [c] Reference 17.

where even slight misorientation of chain axes produces a precipitous drop in stiffness. Previous studies in which corrections were attempted for degree of crystallinity and crystallite orientation yielded values for the axial modulus of 110 ± 10 GPa[10] and 118 GPa,[17] in closer accord with the theoretical upper limit yielded by the model calculation. The discrepancies in C_{11} and C_{12} are more difficult to explain. However, the agreement in the shear constant C_{66} is much better, suggesting that the source of discrepancy arises in C_{11}, C_{22}, and C_{12} in comparable fashion, and may be due to imperfect lateral elastic coupling and a thin amorphous layer between the hot-compacted fibers.

The isothermal elastic compliance matrices may be determined indirectly by inverting the computed stiffness matrices, $\mathbf{S} = \mathbf{C}^{-1}$, or directly by using applied stresses. In this case the agreement with the experimental measurements of Hine and Ward is more satisfying, as shown in Table 4. However, these values must be treated with caution. The triclinic nature of the PET lattice results in significant coupling between diagonal and off-diagonal components, and small numerical errors in off-diagonal matrix elements can lead to large errors upon matrix inversion. The lateral Young's moduli, $E_i = 1/S_{ii}$ (i = 1, 2), and shear moduli, $G_{i-3} = 1/S_{ii}$ (i = 4, 5, 6), determined from the computed elastic stiffness matrices, indicate weak or positive correlations with increasing temperature, a behavior for which there are no data in the literature to confirm.

The stiffness for a single chain computed using the current self-consistent lattice dynamic method at 0 K is 190 GPa. This value is comparable to that of the chain axis in the crystal (204 GPa). This suggests that there is little influence of the chain packing on deformation along the chain axis, similar to what was observed for polyethylene.[6] However, this result contrasts with our previous observations[15,18] and those of Yang and Hsu[19] for poly(p-phenylene terephthalamide), another aromatic polymer, where it was noted that the chain axis modulus in the crystal was significantly higher than that of the single chain. In that case, the difference was traced to the interlocking nature of the aromatic rings of neighboring chains in the lattice; in PET the chain conformation is essentially planar, with no interlocking between neighboring chains.

Previous attempts to estimate the theoretical elastic constants of PET have been confined to calculations of the single-chain stiffness and the axial stiffness of the crystal. Early theoretical estimates of chain stiffness based on single-chain calculations include values of 122 GPa by Treloar[20] and 95 GPa by Tashiro et al.;[21] the latter used a force field parameterized to fit the experimentally measured vibration spectrum of PET. More recently, single-chain estimates of 198 and 244 GPa have been reported by Nicholson et al.,[22] computed respectively using a molecular mechanics calculation with the Dreiding force field[23] and a semiempirical calculation with Mopac using the AM1 model.[24,25] The higher value of stiffness suggested by the semiempirical calculation is consistent with the conclusion, based on polyethylene, that semiempirical methods overestimate modulus by roughly 20%.[26] Alemán and Muñoz-Guerra[27] reported a value for 160 GPa for the single-chain stiffness using molecular mechanics and the AMBER force field[28] with parameters customized for PET. For the PET crystal, Nicholson et al. have further computed a theoretical axial modulus E_3 of 157 GPa and a stiffness C_{33} of 190 GPa, using molecular mechanics with the Dreiding force field. From a similar calculation Alemán and Muñoz-Guerra report a value of 169 GPa. While the Dreiding results are fairly consistent with the results presented here, the AMBER-based results of Alemán and Muñoz-Guerra for stiffness are roughly 15% lower. In that study, the investigators modified the AMBER force field based on semi-empirical AM1 calculations for model compounds. The resulting force field neglected valence cross terms and employed torsional potentials based on the identity of only the two atoms defining the bond about which the torsion occurs, giving a torsional behavior which is averaged with respect to displacement of the atoms bonded to the two defining atoms. It has also been shown that the AM1 method consistently underestimates rotational barriers in conjugated molecules, and in aromatic polyesters in particular.[29−31]

(c) Thermal Expansion and Thermal Stress. The variations with temperature of the lattice constants, as might be measured by X-ray diffraction, for temperatures greater than 50 K may be approximated by fourth-order polynomials, exclusive of the linear term so as not to violate the third law of thermodynamics, fit to the lattice constants, a, b, and c. The resulting equations, from the first derivatives of which the thermal expansion of the lattice may be determined, are

$$a(T) = 4.4259 + 8.01 \times 10^{-7}T^2 - 0.23 \times 10^{-9}T^3 - 9.98 \times 10^{-12}T^4;\ r = 0.9982$$

$$b(T) = 5.9915 + 6.50 \times 10^{-7}T^2 - 1.57 \times 10^{-9}T^3 + 1.95 \times 10^{-12}T^4;\ r = 0.9980$$

$$c(T) = 10.880 - 6.65 \times 10^{-7}T^2 + 2.23 \times 10^{-9}T^3 - 2.96 \times 10^{-12}T^4;\ r = 0.9996$$

$$V(T) = 212.7 + 1.44 \times 10^{-4}T^2 - 3.60 \times 10^{-7}T^3 + 3.95 \times 10^{-4}T^4;\ r = 0.9999 \quad (7)$$

A somewhat more in-depth analysis of the thermal expansion of the triclinic PET unit cell may be accomplished through determination of each of the components of the thermal expansion tensor computed between 50 and 400 K. Each of the six independent parameters of the lattice tensor, $\mathbf{h} = [\mathbf{a}, \mathbf{b}, \mathbf{c}]$, were approximated independently by fourth-order polynomials fit to the values obtained at 50 K intervals between 0 and 400 K. These polynomials were then differentiated to estimate the components of the tensor $\mathrm{d}\mathbf{h}/\mathrm{d}T$ at each temperature. The thermal expansion tensor is then determined using the relation

$$\alpha = \frac{1}{2}\left[\mathbf{h}^{t,-1}\frac{\mathrm{d}\mathbf{G}}{\mathrm{d}T}\mathbf{h}^{-1}\right]$$

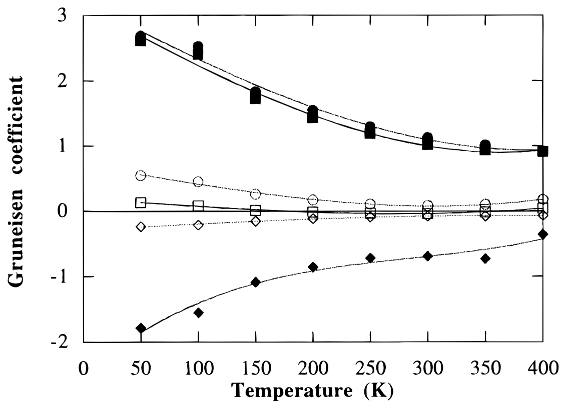

Figure 5. Grüneisen coefficients for the PET crystal as functions of temperature (Voigt notation): γ_1 (filled circles); γ_2 (filled squares); γ_3 (filled diamonds); γ_4 (open circles); γ_5 (open squares); γ_6 (open diamonds).

Table 5. Thermal Expansion and Grüneisen Coefficients Calculated at Several Temperatures

	100 K	200 K	300 K	400 K
α_1 ($\times 10^{-5}$ K^{-1})	7.13	9.80	11.4	15.0
α_2 ($\times 10^{-5}$ K^{-1})	2.72	3.50	4.12	6.36
α_3 ($\times 10^{-5}$ K^{-1})	−0.72	−0.85	−1.07	−2.00
α_4 ($\times 10^{-5}$ K^{-1})	4.65	4.83	4.50	7.60
α_5 ($\times 10^{-5}$ K^{-1})	4.71	−0.63	−1.38	9.06
α_6 ($\times 10^{-5}$ K^{-1})	0.65	2.09	5.05	4.38
γ_1	2.53	1.55	1.13	0.90
γ_2	2.40	1.43	1.02	0.91
γ_3	−1.55	−0.86	−0.69	−0.36
γ_4	0.45	0.17	0.08	0.17
γ_5	0.08	−0.02	−0.04	0.04
γ_6	−0.21	−0.12	−0.08	−0.07
C_V (kcal mol^{-1} K^{-1})	0.0167	0.0334	0.0470	0.0599

where $\mathbf{G}$ is the metric tensor, $\mathbf{h}^t\mathbf{h}$, and $d\mathbf{G}/dT = [\mathbf{h}^t(d\mathbf{h}/dT) + (d\mathbf{h}/dT)^t\mathbf{h}]$. The thermal expansion tensor, α, may be converted to Voigt notation using $\alpha_i = \alpha_{ii}$, $i = 1-3$, and $\alpha_k = 2\alpha_{ij}$, $k = 4-6$, $i \neq j$. These values for thermal expansion of PET are provided in Table 5. The results confirm thermal contraction along the chain direction with increasing temperature for the fully extended PET chain conformation and thermal expansion lateral to this direction. The lateral expansion appears to be significantly anisotropic. α_5 is positive at low temperatures and exhibits a pronounced minimum near 200 K. In this triclinic lattice, this is indicative of competitive influences between expansion along the a-axis, decrease in β and increase in γ with rise in temperature. Similar behavior has been observed for thermal expansion along the chain direction in poly(oxymethylene).[32]

Since thermal expansion may be thought of as a mechanical response to thermally induced stress, one can write

$$\alpha = \frac{C_v}{V}\mathbf{S}\gamma$$

where γ is the vector of Grüneisen coefficients for the lattice, and the components $(C_V/V)\gamma_i$ are the thermal stresses. The specific heat of PET at constant volume between 100 and 400 K is shown in Table 5. Using eq 9 the lattice Grüneisen coefficients were determined and reported in Table 5 at several temperatures. Their temperature dependencies are illustrated in Figure 5. As has been observed in previous investigations of other polymers, most of the γ_i are positive over the entire temperature range, consistent with entropically driven lattice expansion. γ_3 is negative over the entire temperature range, indicating an entropically driven contraction of the lattice in the chain direction. This behavior is in accord with our observations for other crystal forms with fully extended chain conformations. γ_6 is also found to be small and negative over the entire temperature range. These two contributions account for roughly 75% of the negative α_3 at 300 K. The results for thermal expansion and Grüneisen coefficients are consistent with results for other polymers and lend some credibility to the elastic compliances, S_{ij}, computed by inversion of the stiffness matrix, and to their unusual temperature dependence.

Conclusion

The thermomechanical properties of PET between 0 and 400 K have been computed within the quasiharmonic approximation using a consistent formulation of lattice dynamics which relies entirely on the accuracy of the input force field for both lattice dimensions and vibrational frequencies. This is the first report of the fully anisotropic behavior for PET. The good agreement between the computed and observed lattice constants and vibrational frequencies at 300 K support the validity of the pcff force field for this aromatic polyester, at least for the conformation observed in the crystalline state. Knowledge of the vibrational frequencies and their associated polarization vectors allows direct estimation of the mean square displacement matrices for each atom, which is important in estimating the atomic B-factors and the reduction in Bragg intensities due to thermal diffuse scattering in empirical wide-angle X-ray measurements. One advantage of so doing is to quantify the degree of crystal imperfection in laboratory samples from X-ray measurements. Furthermore, these vibrations reveal a clear picture of translational oscillations of the chain along three orthogonal axes and libration of the chain about its axis.

The computed elastic constants are in accord with the available estimates from previous computations and with empirical data. As is commonly the case, the theoretical chain stiffness is about 50% higher than that estimated by the X-ray method. There are no empirical data available for comparison to the remaining elastic properties. However, for the fully oriented, crystalline composite with transverse isotropy we compute elastic stiffnesses in fair agreement with the best data available from ultrasonic velocity measurements on hot-compacted PET fibers. The experimental values are expected to be somewhat less than the theoretical values, due to less than 100% crystallinity and imperfect orientation of the crystallites in the hot-compacted material.

The thermal expansion behavior of the PET crystal lattice has been computed for the first time from molecular-level interactions. The temperature dependencies of the lattice constants, a, b, and c, as well as their Cartesian components were fit using fourth-order polynomials, providing detailed analytical expressions for thermal expansion over a range of temperatures. For the crystallographic parameters a, b, and c, these expressions could be checked by appropriate X-ray diffraction measurements. By fitting the individual components of the lattice tensor separately, one can construct the thermal expansion tensor at any temperature and compute the corresponding thermal stresses. Previously, these thermal stresses were estimated from the change in entropy with small, finite strain.[6] These resulting Grüneisen coefficients and their temperature dependencies are comparable to those observed for other polymer crystals with extended chain conformations. In addition to finding γ_3 to be negative at all temperatures, a second Grüneisen coefficient, γ_6, is also found to be negative.

Acknowledgment. The author is grateful to the National Science Foundation for financial support (Grant CTS-9457111) during the course of this work

References and Notes

(1) Fu, Y.; Annis, B.; Boller, A.; Jin, Y.; Wunderlich, B. *J. Polym. Sci., Polym. Phys.* **1994**, *32*, 2289.
(2) Ajji, A.; Guèvremont, J.; Cole, K. C.; Dumoulin, M. M. *Polymer* **1996**, *37* (16), 3707.
(3) Discover User Guide, version 2.3.7, Biosym Technologies, San Diego, 1994.
(4) Sun, H. *J. Comput. Chem.* **1994**, *15* (7), 752.
(5) Karasawa, N.; Goddard, W. A. *J. Phys. Chem.* **1989**, *93*, 7320.
(6) Lacks, D. J.; Rutledge, G. C. *J. Phys. Chem.* **1994**, *98*, 1222.
(7) Lacks, D. J.; Rutledge, G. C. *J. Chem. Phys.* **1994**, *101*, 9961.
(8) Daubeny, R. de P.; Bunn, C. W.; Brown, C. J. *Proc. R. Soc. London* **1954**, *A226*, 531.
(9) Kitano, Y.; Kinoshita, Y.; Ashida, T. *Polymer* **1995**, *36* (10), 1947 and references therein.
(10) Thistlethwaite, T.; Jakeways, R.; Ward, I. M. *Polymer* **1988**, *29*, 61 and references therein.
(11) Karasawa, N.; Goddard, W. A. *J. Phys. Chem.* **1991**, *95*, 2260.
(12) Boerio, F. J.; Bahl, S. K.; McGraw, G. E. *J. Polym. Sci., Polym. Phys.* **1976**, *14*, 1029.
(13) Burnett, M. N., Johnson, C. K. Ortep-III: Oak Ridge Thermal Ellipsoid Plot Program for Crystal Structure Illustrations, Oak Ridge National Laboratory Report ORNL-6895, 1996.
(14) Willis, B. T. M.; Pryor, A. W. *Thermal Vibrations in Crystallography*, Cambridge University Press: Cambridge, 1975.
(15) Rutledge, G. C., Suter, U. W. *Polymer* **1991**, *32*, 2179.
(16) Hine, P. J.; Ward, I. M. *J. Mater. Sci.* **1996**, *31*, 371.
(17) Matsuo, M.; Sawatari, C. *Polym. J.* **1990**, *22* (6), 518.
(18) Lacks, D. J., Rutledge, G. C. *Macromolecules* **1994**, *27*, 7197.
(19) Yang, X.; Hsu, S. L. *Macromolecules* **1991**, *24*, 6680.
(20) Treloar, L. R. G. *Polymer* **1960**, *1*, 279.
(21) Tashiro, K.; Kobayashi, M.; Tadokoro, H. *Macromolecules* **1977**, *10*, 413.
(22) Nicholson, T. M., Davies, G. R., Ward, I. M. *Polymer* **1994**, *35* (20), 4259.
(23) Mayo, S. L.; Olafson, B. D.; Goddard, W. A. *J. Phys. Chem.* **1990**, *94*, 8897.
(24) Stewart, J. J. P. *J. Computer-Aided Mol. Des.* **1990**, *4*, 1.
(25) Dewar, M. J. S.; Zoebisch, E. G., Healy, E. F.; Stewart, J. J. P. *J. Am. Chem. Soc.* **1985**, *107*, 3902.
(26) Crist, B.; Hereña, P. G. *J. Polym Sci., Polym. Phys.* **1996**, *34* (3), 449.
(27) Alemán, C., Muñoz-Guerra, S. *J. Polym. Sci., Polym. Phys.* **1996**, *34*, 963.
(28) Weiner, S. J.; Kollman, P. A.; Case, D. A.; Singh, U. C.; Ghio, C.; Alagona, G. *J. Am. Chem. Soc.* **1984**, *106*, 765. Weiner, S. J.; Kollman, P. A.; Nguyen, D. T.; Case, D. A. *J. Comput. Chem.* **1990**, *7*, 230.
(29) Fabian, W. *J. Comput. Chem.* **1988**, *9*, 369.
(30) Coussens, B.; Pierloot, K.; Meier, R. J. *J. Mol. Struct. THEOCHEM* **1992**, *259*, 331.
(31) Alemán, C.; Julia, L. *J. Phys. Chem.* **1996**, *100*, 1524.
(32) White, G. K.; Smith, T. F.; Birch, J. A. *J. Chem. Phys.* **1976**, *65*(2), 554.

MA961800Q